Analytica Chimica Acta 1122 (2020) 70–75

Contents lists available at ScienceDirect

Analytica Chimica Acta

journal homepage: www.elsevier.com/locate/aca

Boron-doped diamond electrochemical aptasensors for trace aflatoxin B_1 detection

Zhiyuan Feng , Nan Gao , Junsong Liu , Hongdong Li *

State Key Lab of Superhard Materials, College of Physics, Jilin University, Changchun, 130012, PR China

HIGHLIGHTS

- An electrochemical aptasensor based on boron-doped diamond is designed.
- The aptasensor is highly sensitive and specific to trace aflatoxin B1 detection.
- The aptasensor shows high stability, repeatability, reusability and practivability.

GRAPHICAL ABSTRACT

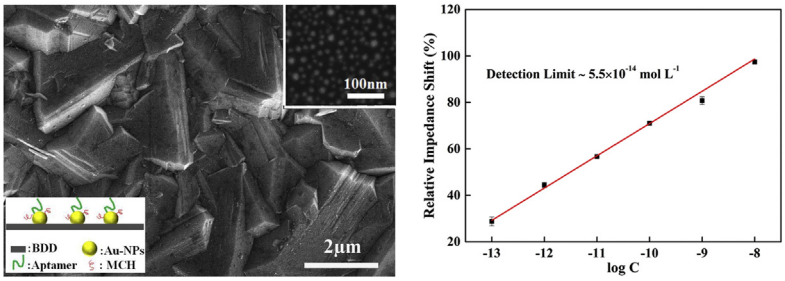

ARTICLE INFO

Article history:
Received 21 December 2019
Received in revised form
23 April 2020
Accepted 24 April 2020
Available online 27 April 2020

Keywords:
Electrochemical aptasensor
Aflatoxin B_1
Low detection limit
Boron-doped diamond

ABSTRACT

An electrochemical aptasensor for detecting trace aflatoxin B_1 (AFB_1) is designed and fabricated consisting of aptamers and gold nanoparticles on conductive boron-doped diamond (BDD) electrode. By examining the relative impedance shift from electrochemical impedance spectroscopy as a function of AFB_1 concentration, the low detection limit (wide linear relationship range) of the aptasensor is realized to be 5.5×10^{-14} mol L^{-1} (1.0×10^{-13}–1.0×10^{-8} mol L^{-1}). The variation in impedance property of the aptasensor is determined by the specific adsorption of AFB_1 molecules to the aptamer at a certain concentration covering the electrode. By means of multiple characteristic processes, it is demonstrated that the constructed aptasensor is favorable for testing the trace AFB_1 with high specificity, sensitivity, stability, repeatability, and reusability, which lead to a possibility to achieve high performance biosensor for practical application to quantitatively detract trace AFB_1 in environments.

1. Introduction

Being the toxic secondary metabolites produced by fungi, the mycotoxins are ubiquitous in food, feed and environment, which are injurious to human and animal health upon ingestion, inhalation, or skin contact [1,2]. The aflatoxins are one of the most relevant groups of mycotoxins found in food, which have strong toxicity and exist everywhere. At present, there are four kinds of aflatoxins, aflatoxin B_1 (AFB_1), aflatoxin B_2 (AFB_2), aflatoxin G_1 (AFG_1), aflatoxin G_2 (AFG_2), and two additional metabolites of aflatoxin M_1 (AFM_1) and aflatoxin M_2 (AFM_2) [3]. Among them, AFB_1 widely exists in the moldy human food and animal feed, which can lead to hepatic cancer and even death, and AFB_1 is thus categorized as a first-grade carcinogen [4,5]. Moreover, AFB_1 is heat-resistant with a cracked temperature higher than 268 °C, and may survive in regular cooking procedures [6]. The European Union sets a limit of 2.0 μg/kg (6.4 nM) on AFB_1 in peanuts, and nuts and their processed products [7]. Thus, an effective technique to detect trace AFB_1 is necessary.

* Corresponding author.
E-mail address: hdli@jlu.edu.cn (H. Li).

https://doi.org/10.1016/j.aca.2020.04.062
0003-2670/

The typical techniques, such as thin-layer chromatography [8,9], high-performance liquid chromatography [10,11], and enzyme-linked immunosorbent method [12,13] have been developed to detect AFB_1. The detection limit of these techniques is from 10^{-9} to 10^{-7} mol L^{-1} (Table 1). However, some methods (for example, the gas chromatography [14] and liquid chromatography [15]) are high cost and have complex procedures far from fulfilling modern detection requirements. Recently, electrochemical method had attracted more attentions to detect trace AFB_1, due to its advantages of easy operation, high sensitivity and selectivity, low reagent consumption, wide dynamic range, low detection limit, and low cost [16,17]. Several kinds of electrochemical sensors have been reported based the electrodes of glassy carbon [18], screen printed bipolar electrode [19], and carbon nanotubes [20]. Importantly, aptamer was introduced on the electrochemical electrode to significantly increase the specificity and sensitivity of the sensors [21–26], as shown in Table 1. Although detection limit of AFB_1 can reach as low as 10^{-9} to 10^{-14} mol L^{-1}, the related poor repeatability and narrow detection range of these AFB_1 sensors degraded the applications of these sensors.

It is known that boron-doped diamond (BDD) has been widely employed as an important electrode material to fabricate high performance electrochemical sensors, because of its wide potential window, chemical inertness, low resistance, mechanical rigidity, and low background current [27–29], which have been applied as the electrode material to construct high-performant electrochemical aptasensor [30–32]. However, there are a few BDD-related electrochemical sensors reported to detect trace AFB_1 in previous literature. In this paper, an aptasensor, consisting of BDD electrode modified with Au nanoparticles (Au-NPs), aptamers, and 6-mercapto-1-hexanol (MCH), is designed and performed to detect AFB_1. By testing the relative impedance shift at varying AFB_1 concentration, a low detection limit of 5.5×10^{-14} mol L^{-1} and a wide linear relationship range of 1.0×10^{-13}–1.0×10^{-8} mol L^{-1} are realized, showing high specificity and sensitivity for AFB_1 detection. The stability, repeatability, and reusability of the aptasensors are examined. Moreover, the aptasensor can precisely detect the AFB_1 concentration in minced peanut powder.

2. Experimental section

2.1. Procedures

The design and manufacturing process of MCH/Aptamers/Au-NPs/BDD (MAABD) aptasensors are presented in Fig. 1 and Fig. S1.

2.1.1. Preparation of MAABD electrodes

The polycrystalline BDD films were deposited on p-type silicon (100) substrates by microwave plasma chemical vapor deposition (MPCVD) method (Fig. S1a). Then, a thin Au layer (thickness of about 25 nm) was sputtered on the BDD surface (Fig. S1b). The Au-NPs/BDD electrode was thermally treated in air at 800 °C for 1 min to form Au-NPs by a dewettability process (Fig. S1c). The aptamer selected is a class of single-stranded oligonucleotide that could bind specifically to the target of AFB_1 with a base sequence of 5′-SH-$(CH_2)_6$-GTT GGG CAC GTG TTG TCT CTC TGT GTC TCG TGC CCT TCG CTA GGC CCA CA-3′ [33]. After modification of 5′-end of the aptamer with a mercapto group for 12 h at 37 °C, the aptamer was bonded to Au-NPs by the Au–S bonds to construct the aptamers/Au-NPs/BDD (AA/BDD) electrode (Fig. S1d). After cleaning in deionized water, the AA/BDD electrodes were soaked in a 1 μmol L^{-1} MCH, and assembled at room temperature for 1 h. The MCH molecules were adsorbed on the surfaces of AA/BDD electrodes with aptamer covering (Fig. S1e). MCH/aptamers/Au-NPs/BDD (MAABD) aptasensors were then fabricated after being washed with phosphate buffer saline (PBS) (Fig. S1f).

2.1.2. Electrochemical tests and detection of AFB_1

The electrochemical tests were carried out in a mixed electrolyte containing 5 mmol L^{-1} $Fe(CN)_6^{3-}/Fe(CN)_6^{4-}$ redox probe and 0.1 mol L^{-1} KCl. Electrochemical impedance spectroscopy (EIS) measurements were carried out at perturbation amplitudes at sinusoidal voltages of 5 mV and frequency of 10^{-2} to 10^{5} Hz.

The MAABD aptasensors were employed to detect AFB_1 concentrations in PBS. The AFB_1 were added to PBS by the standard addition method to prepare PBS with AFB_1 at various concentrations. In a typical AFB_1 detection process, a MAABD aptasensor was immersed in PBS containing AFB_1 at a certain concentration for 15 min, and then taken out to be rinsed with deionized water to remove non-specific absorbed AFB_1. From EIS measurements, the cleared aptasensor was measured in the electrolyte. Before each procedure, a measurement of R_{ct0} (initial impedance value of the bare aptasensor) was carried out firstly. The relative impedance shift (RIS) was defined by $(R_{ct}-R_{ct0})/R_{ct0}$, where R_{ct} is the impedance value after the aptasensor contacted AFB_1, and the RIS is dependent on the AFB_1 concentration. For the next measurement using the same aptasensor, the electrode (rinsed with Ethylene Diamine Tetraacetic Acid (EDTA)) was immersed in PBS containing AFB_1 at a certain concentration for 15 min, then rinsed with deionized water followed by measurement in the electrolyte containing the redox probe and KCl. After detection and recycling, an aptasensor was used to detect the different concentrations of AFB_1.

Table 1
The detection limit and linear range of aflatoxin B_1 (AFB_1) detection by various methods.

Methods	Detection limit (M)	Linear range (M)	References
thin layer chromatography	3.2×10^{-9}	6.4×10^{-9}–3.2×10^{-8}	[8]
liquid chromatography	1.3×10^{-7}	1.3×10^{-7}–3.8×10^{-7}	[10]
enzyme-linked immunosorbent	3.2×10^{-10}	1.3×10^{-8}–1.9×10^{-7}	[12]
Electrochemistry:silica gel–ionic liquid biocompatible film	3.2×10^{-11}	3.2×10^{-10}–3.2×10^{-8}	[17]
electrochemistry:polythionine/gold nanoparticles	2.2×10^{-10}	1.9×10^{-9}–7.7×10^{-9}	[18]
electrochemistry:96-well screen-printed microplate	9.6×10^{-11}	1.6×10^{-10}–6.4×10^{-9}	[19]
electrochemistry:single-walled carbon nanotubes/chitosan	1.1×10^{-11}	3.2×10^{-11}–3.2×10^{-7}	[20]
EA: complementary DNA	2.0×10^{-9}	2.0×10^{-9}–4.0×10^{-6}	[21]
EA: fluorescent ternary CdZnTe quantum dots	6.4×10^{-11}	1.6×10^{-10}–3.2×10^{-7}	[22]
EA: real time polymerase chain reaction	8.0×10^{-14}	1.6×10^{-12}–1.6×10^{-7}	[23]
EA: semiconductor quantum dots	1.4×10^{-11}	1.6×10^{-11}–1.6×10^{-7}	[24]
EA: ferrocene/β-cyclodextrin	1.6×10^{-14}	3.2×10^{-13}–3.2×10^{-8}	[25]
EA: graphene oxide/aptamer multi-anodized anodized aluminum	4.2×10^{-10}	3.2×10^{-9}–6.4×10^{-8}	[26]
EA: MCH/Aptamers/Au-NPs/BDD	5.5×10^{-14}	1.0×10^{-13}–1.0×10^{-8}	This work

Abbreviation: EA (electrochemical aptasensor).

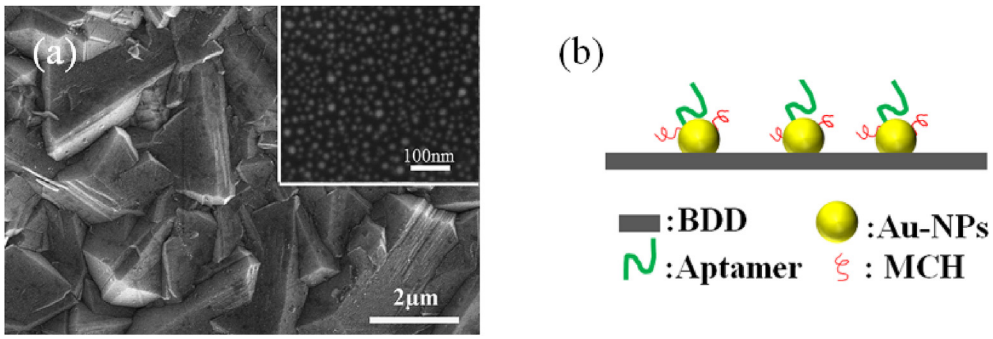

Fig. 1. (a) SEM images of the BDD film and Au-nanoparticles (Au-NPs) on the film. The inset of (a) is the high-magnitude image of Au-NPs. (b) Schematic diagram of the aptasensor structure consisting of BDD, Au-NPs, aptamer, and MCH.

The sample of trace AFB_1 in peanut samples was fabricated and detected. Fresh peanut samples purchased from a local market were ground first. The ground peanut powder (6 g) were added to PBS, and then treated with ultrasonic shock for 15 min, followed by centrifugation for 10 min. The whey solution was taken for filtration. The 20 mL PBS with varying concentrations of AFB_1 was prepared by standard addition method.

2.2. Characterization and electrochemical measurements

The surface morphology and crystal structure were characterized by scanning electron microscopy (SEM, FEI magellan 400) equipped with an energy-dispersive X-ray spectrometer (EDS, OXFord Max 150). X-ray diffraction technique (XRD, RigakuD/Max-RA), and Raman spectroscopy (Renishaw in Via Raman microscope equipped with 532 nm laser excitation). All electrochemical tests were performed at room temperature in a three-electrode system of an electrochemical workstation (CHI 760 E). BDD electrodes with a geometric area of 0.21 cm^2 were used as working electrodes, a platinum wire as the auxiliar electrode, and a saturated calomel electrode as the reference electrode in the electrochemical tests.

3. Results and discussion

3.1. Characterization of Au-NPs/BDD electrodes

Observed from SEM images (Fig. 1a and Fig. S2a), the polycrystalline BDD films are mainly composed of (111) and (110) grains with average size of 1.8 μm, which is consistence with the XRD result (Fig. S3a). The Raman spectrum of the BDD films shows the asymmetric characteristic diamond band at ~1330 cm^{-1} and the broad peak centered at ~1200 cm^{-1}, which is attributed to the Fano effect and increased density of states by heavy boron doping of about 10^{20} cm^{-3} resulting in metallic type conductivity of BDD [34]. The Au-NPs with an average size of ~13 nm are uniformly deposited on the BDD surfaces, with a density of about 3.2×10^{11} cm^{-2} (Fig. 1a and Fig. S2b). The presence of Au NPs on the BDD films is further confirmed EDS element mapping (Fig. S2c).

3.2. Electrochemical impedance characterization of MAABD aptasensor

In Fig. 2a, the impedance of the BDD electrodes (425 Ω) decreases to 166 Ω for the Au-NPs/BDD electrodes, indicating that the introduction of Au-NPs improves the conductivity, due to the enhanced electron transfer of Au-NPs [35,36]. After the aptamers are modified on Au-NPs/BDD electrodes, the impedance value greatly increases to 1367 Ω, due to the electrostatic repulsion between the negatively charged aptamer and the $Fe(CN)_6^{3-/4-}$ redox probe on the Au-NPs/BDD electrode surface [37]. When AFB_1 molecules contact the aptasensor surface, the aptamer will specifically adsorb the AFB_1 forming a surface spatial conformation, which will hinder Fe^{3-} and Fe^{4-} ions transferring in the electrolyte near the electrode surface, and then the electrode impedance would increase. With further increasing the adsorption of AFB_1, the coverage of AFB_1 on electrode enhances gradually, resulting in the increase of impedance of electrode. In a certain examination region, the impedance values linearly increase dependent on the increase of AFB_1 concentration.

By adding MCH to the AA/BDD surfaces, the impedance value increases to 3002 Ω, because MCH further prevents the redox probe from attaching to the conductive Au-NPs/BDD electrode. In Fig. 2b, for the response of AFB_1 on various electrodes, the impedance signals from BDD electrodes and Au-NPs/BDD electrodes with and without AFB_1 are nearly the same, indicating the electrodes are not responsive to AFB_1. It is noted that increase of impedance for MAABD sensor is significant with adding AFB_1 with respect to the case of without AFB_1, which is more sensitive than that for AA/BDD sensor. Therefore, the aptasensor of MAABD is suitable for detecting trace AFB_1 with high sensitivity.

3.3. MAABD aptasensors for AFB_1 detection

Fig. 3a shows the impedance spectra of the MAABD electrodes exposed to AFB_1 at different concentrations. The impedances are obtained using the equivalent circuit (the inset of Fig. 3a). In Fig. 3b, the RIS increases linearly with increasing AFB_1 concentration in the region of 1.0×10^{-13}–1.0×10^{-8} mol L^{-1}, following the equation of $I = I_0 + AlogC$, where I is RIS, and C is the AFB_1 concentration, I_0 and A are the fitting parameters. The fitted I_0 (A) is 209.84 (13.89), and the correlation coefficient (R^2) is 0.997. The detection limit of the MAABD aptasensors is calculated according to the response of three standard deviations of zero concentration-response based on the equation of $3S = I_0 + AlogC$, where S is standard deviation [30,38]. The standard deviation of a blank sample on an aptasensor is relative standard deviation (RSD) = 0.15%, n = 3. The detection limit of the aptasensor for AFB_1 is estimated to be 5.5×10^{-14} mol L^{-1}, which is relatively lower than most previous reports by various detection methods, as listed in Table 1.

The high performance MAABD electrodes for AFB_1 detection can be explained from the following aspects. First, the conductive BDD electrode has wide potential window, excellent structural stability, low background current, and fouling resistance, which could enhance the detection performance and significantly reduce the background signals and various interferences from the electrode. However, for most other substrates (i.e., glassy carbon [18], carbon

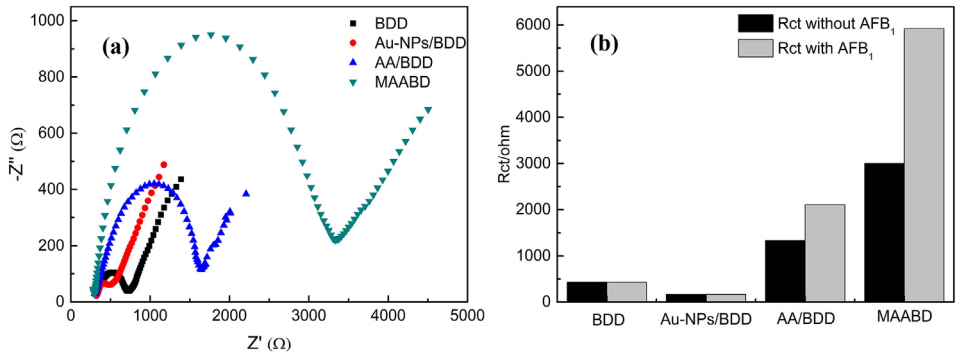

Fig. 2. (a) Impedance spectra (Nyquist plots) of BDD, Au-NPs/BDD, AA/BDD and MAABD electrodes tested in 5 mmol L^{-1} $Fe(CN)_6^{3-/4-}$ solution containing 0.1 mol L^{-1} KCl, showing the variations of impedance dependent on the corresponding structures. (b) Bar graph of impedance variation of the four detectors incubated in the redox probe/KCl electrolyte with and without AFB_1 at a concentration of 10^{-8} mol L^{-1}, for comparison.

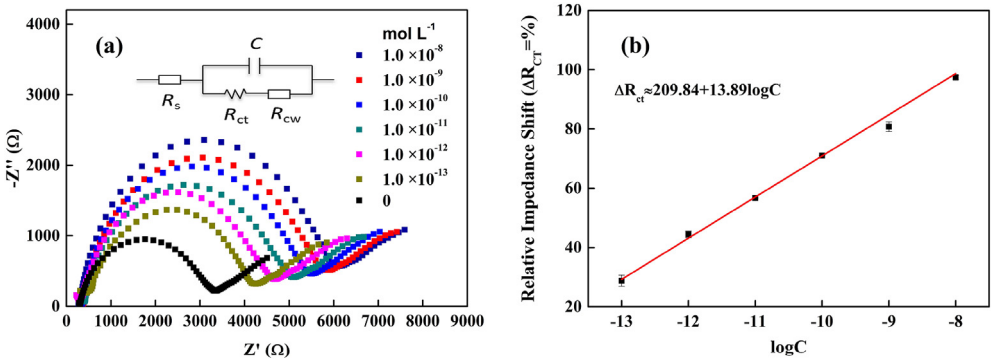

Fig. 3. (a) Impedance spectra (Nyquist plots) of MAABD aptasensor incubated at AFB_1 concentrations in the region of 1.0×10^{-13}–1.0×10^{-8} mol L^{-1} measured in redox probe/KCl electrolyte, for comparison. The inset in (a) is the equivalent circuit of impedance. (b) The calibration plot of relative impedance shift (RIS, ΔR_{ct}) as a function of AFB_1 concentration following a linear relation.

tubes [20]), their intrinsic narrow potential window, unstable surface and strong background signal would interfere with the signals of AFB_1. Secondly, after Au-NPs were sputtered on the BDD film, the surface area of Au-NPs/BDD electrode (0.88 cm^2 estimated by cyclic volt-ampere method [30]) is three times that of BDD electrode (0.28 cm^2). The cyclic volt-ampere results (Fig. S4) suggest that the Au-NPs/BDD could provide more active sites for bonding oligonucleotide aptamers [39]. At the meantime, the impedance of the Au-NPs/BDD electrodes decreases to a certain content (Fig. 2a). Third, the aptamers screened by exponential enrichment (SELEX) have better specific binding to AFB_1 [40]. The detection limit was further extended to lower levels. Finally, the absorbed MCH molecules can hold the aptamers and arrange the aptamers vertically on the electrode surfaces to capture more AFB_1 molecules [32], and furthermore, the MCH molecules can occupy the redundant active sites without aptamers on Au-NPs and BDD surfaces, which can effectively reduce the non-specific adsorption [30,41].

The specificity of the aptasensors for AFB_1 detection was examined by introducing some selected interferences having similar structure to AFB_1. The aflatoxin B_2 (AFB_2), aflatoxin G_1 (AFG_1), aflatoxin G_2 (AFG_2), and mixture of (AFB_2 + AFG_1 + AFG_2) were respectively added into the solutions having AFB_1 at a concentration of 5.0×10^{-9} mol L^{-1}, and the concentrations for those mixtures are 100 times that of the AFB_1. The relative impedance response was measured for the specificity of MAABD aptasensors (Fig. 4a). The initial impedance of the pure AFB_1 is set as the standard, and experimentally, the corresponding percentage change of impedance for those mixed solutions measured are as low as −2.1%–2.8%, meaning a high specificity of AFB_1 for MAABD aptasensors realized. The examinations of individual AFB_1, AFB_2, AFG_1, and AFG_2 on the aptasensors (Fig. S5) further verify the above conclusion.

In addition, the stability of the blank MAABD aptasensors was tested by a relative impedance response in $Fe(CN)6^{3-/4-}$/KCl electrolyte. In the process, the test on the first day is performed as the 1st cycle, and then the aptasensor was cleaned by PBS and deionized water to be stored in a refrigerator at 4 °C. After 24 h interval, the same aptasensor was tested under the same condition for the 2nd cycle. Following the same cyclic process, the data from 10 days were collected (Fig. 4b) for the comparison. The fluctuation of relative impedance response for the same aptasensor is within in −3.4%–6.4% corresponding to the standard of 1st cycle, indicating that the MAABD aptasensors have excellent stability feature. Furthermore, in order to examine the repeatability of aptasensors, a recyclable test was carried out during two groups of measurement cycles with removing/re-adsorbing AFB_1 on the cleaned MAABD surface, and shown in Fig. S6. Evidently, an excellent repeatability of the aptasensor is demonstrated for the AFB_1 detection.

3.4. Detecting the recovery rate of AFB_1 in real sample

To test the potential practical application of the MAABD aptasensor, the detection examination was performed on a minced peanut powder sample with adding AFB_1 at various concentrations. In Fig. S7, the impedance has an enhanced shift tendency with increasing the AFB_1 concentration, and a linear relationship is in the region of 1.0×10^{-13}–1.0×10^{-8} mol L^{-1}. The recovery and RSD of the peanut sample with varying AFB_1 concentrations

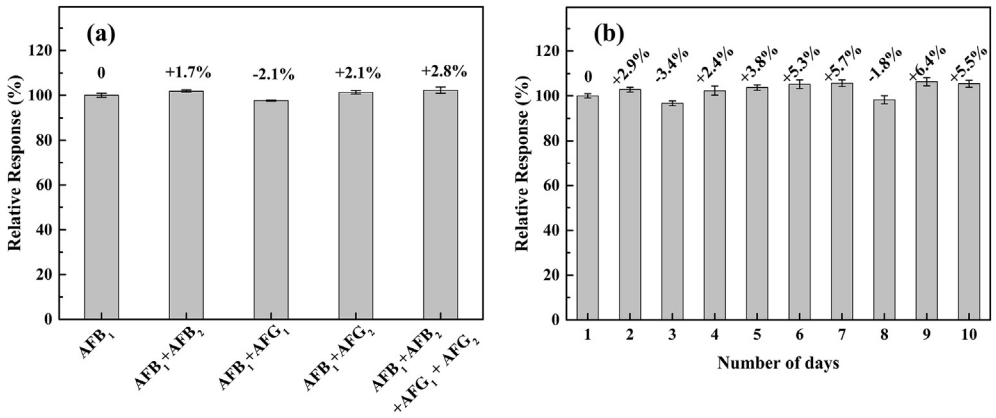

Fig. 4. Bar graph of relative impedance responses of MAABD aptasensor for the cases of (a) incubated with different interferences to AFB_1, measured in redox probe/KCl electrolyte, for comparison to test the specificity MAABD aptasensor, (b) examined in 5 mmol L^{-1} $Fe(CN)_6^{3-/4-}$ solution containing 0.1 mol L^{-1} KCl from 1st to 10th day to test the stability of MAABD aptasensor. The fluctuations of relative impedance response corresponding to the set standard are presented above bars for different cases.

Table 2
Recovery and relative standard deviation (RSD) of AFB_1 tested at different concentrations in peanut powders.

Samples	Added AFB_1 (mol L^{-1})	Detected (mol L^{-1})	Recovery (%)	RSD (%)
1	0	Undetectable		
2	1.00×10^{-13}	0.96×10^{-13}	96	3.2
3	1.00×10^{-12}	1.09×10^{-12}	109	4.4
4	1.00×10^{-11}	1.04×10^{-11}	104	3.9

(1.0×10^{-13}–1.0×10^{-11} mol L^{-1}) are summarized in Table 2. The recoveries are of 96–109% and the RSD are smaller than 4.4%. This result indicates that the MAABD aptasensor is suitable to detect the trace AFB_1 in some practical samples with high specificity and sensitivity.

4. Conclusions

In this paper, the BDD-based aptasensor was designed and fabricated to detect trace AFB_1. A linear range of 1.0×10^{-13} – 1.0×10^{-8} mol L^{-1} and a detection limit of 5.5×10^{-14} mol L^{-1} have been achieved, showing high sensitivity and specificity for AFB_1 detection. The detection is superior to most previous electrochemical sensors, mainly attributed to the synergistic effect of BDD, Au-NPs, aptamers and MCH. The stability, repeatability, and reusability of the aptasensor are demonstrated. Moreover, the aptasensor is performed to examine the trace AFB_1 in real peanut sample. These results in the work are helpful to construct novel diamond-based sensors to detect various substances with high sensitivity and specificity for environmental pollution detection and monitoring.

Declaration of competing interest

The authors declare that they have no known competing financial interests or personal relationships that could have appeared to influence the work reported in this paper.

CRediT authorship contribution statement

Zhiyuan Feng: Investigation, Formal analysis, Writing - original draft. **Nan Gao:** Formal analysis, Writing - original draft. **Junsong Liu:** Formal analysis. **Hongdong Li:** Conceptualization, Formal analysis, Supervision, Writing - review & editing.

Acknowledgements

This work was financially supported by the National Natural Science Foundation of China (Grant No. 51672102), and the Program for Changjiang Scholars and Innovative Research Team in University (No. IRT 15R23).

Appendix A. Supplementary data

Supplementary data to this article can be found online at https://doi.org/10.1016/j.aca.2020.04.062.

References

[1] D.R. Milicevic, M. Skrinjar, T. Baltic, Real and perceived risks for mycotoxin contamination in foods and feeds: challenges for food safety control, Toxins 2 (2010) 572–592.
[2] B. Wang, Y. Chen, Y. Wu, B. Weng, Y. Liu, Z. Lu, C.M. Li, C. Yu, Aptamer induced assembly of fluorescent nitrogen-doped carbon dots on gold nanoparticles for sensitive detection of AFB1, Biosens. Bioelectron. 78 (2016) 23–30.
[3] G. Castillo, K. Spinella, A. Poturnayová, M. Šnejdárková, L. Mosiello, T. Hianik, Detection of aflatoxin B 1 by aptamer-based biosensor using PAMAM dendrimers as immobilization platform, Food Contr. 52 (2015) 9–18.
[4] A. Bacaloni, C. Cavaliere, F. Cucci, P. Foglia, R. Samperi, A. Lagana, Determination of aflatoxins in hazelnuts by various sample preparation methods and liquid chromatography-tandem mass spectrometry, J. Chromatogr. A 1179 (2008) 182–189.
[5] K.Y. Goud, G. Catanante, A. Hayat, M. Satyanarayana, K.V. Gobi, J.L. Marty, Disposable and portable electrochemical aptasensor for label free detection of aflatoxin B1 in alcoholic beverages, Sensor. Actuator. B Chem. 235 (2016) 466–473.
[6] S. Marin, A.J. Ramos, G. Cano-Sancho, V. Sanchis, Mycotoxins: occurrence, toxicology, and exposure assessment, Food Chem. Toxicol. 60 (2013) 218–237.
[7] Commission regulation (Ec), Off. J. Eur. Union.L77, 1-6.
[8] I. Var, B. Kabak, F. Gök, Survey of aflatoxin B1 in helva, a traditional Turkish food, by TLC, Food Contr. 18 (2007) 59–62.
[9] M. Trucksess, W. Brumley, S. Nesheim, Rapid quantitation and confirmation of aflatoxins in corn and peanut butter, using a disposable silica gel column, thin layer chromatography, and gas chromatography/mass spectrometry, J. Assoc. Off. Anal. Chem 67 (1984) 973–975.
[10] C. Cavaliere, P. Foglia, C. Guarino, M. Nazzari, R. Samperi, A. Lagana, Determination of aflatoxins in olive oil by liquid chromatography-tandem mass spectrometry, Anal. Chim. Acta 596 (2007) 141–148.
[11] L.T. Tuinstra, W. Haasnoot, Rapid determination of aflatoxin B1 in Dutch feeding stuffs by high-performance liquid chromatography and post-column derivatization, J. Chromatogr. A 282 (1983) 457–462.
[12] N. Ramakrishna, J. Lacey, A. Candlish, J. Smith, I. Goodbrand, Monoclonal antibody-based enzyme linked immunosorbent assay of aflatoxin B1, T-2 toxin, and ochratoxin A in barley, J. Assoc. Off. Anal. Chem 73 (1990) 71–76.
[13] D. Lawellin, D. Grant, B. Joyce, Enzyme-linked immunosorbent analysis for aflatoxin B1, Appl. Environ. Microbiol. 34 (1977) 94–96.
[14] T. GoTo, M. Matsui, T. Kitsuwa, Analysis of Aspergillus mycotoxins by gas chromatography using fused silica capillary column, JSM Mycotoxins 1990

(1990) 43–47.
[15] M. Nakajima, H. Tsubouchi, M. Miyabe, Y. Ueno, Survey of aflatoxin B1 and ochratoxin A in commercial green coffee beans by high-performance liquid chromatography linked with immunoaffinity chromatography, Food Agric. Immunol. 9 (1997) 77–83.
[16] P. Gan, D. Lowinsohn, J.S. Foord, R.G. Compton, The measurement of the gibbs energy of transfer between oil and water using a nano-carbon paste electrode, Electroanalysis 26 (2014) 351–358.
[17] Z.J. Li, Z.Y. Wang, X.L. Sun, Y.J. Fang, P.P. Chen, A sensitive and highly stable electrochemical impedance immunosensor based on the formation of silica gel–ionic liquid biocompatible film on the glassy carbon electrode for the determination of aflatoxin B1 in bee pollen, Talanta 80 (2010) 1632–1637.
[18] J.H. Owino, O.A. Arotiba, N. Hendricks, E.A. Songa, N. Jahed, T.T. Waryo, R.F. Ngece, P.G. Baker, E.I. Iwuoha, Electrochemical immunosensor based on polythionine/gold nanoparticles for the determination of aflatoxin B(1), Sensors 8 (2008) 8262–8274.
[19] S. Piermarini, L. Micheli, N.H. Ammida, G. Palleschi, D. Moscone, Electrochemical immunosensor array using a 96-well screen-printed microplate for aflatoxin B1 detection, Biosens. Bioelectron. 22 (2007) 1434–1440.
[20] X. Zhang, C.R. Li, W.C. Wang, J. Xue, Y.L. Huang, X.X. Yang, B. Tan, X.P. Zhou, C. Shao, S.J. Ding, J.F. Qiu, A novel electrochemical immunosensor for highly sensitive detection of aflatoxin B1 in corn using single-walled carbon nanotubes/chitosan, Food Chem. 192 (2016) 197–202.
[21] C. Wang, Y. Li, Q. Zhao, A signal-on electrochemical aptasensor for rapid detection of aflatoxin B1 based on competition with complementary DNA, Biosens. Bioelectron. 144 (2019) 111641.
[22] X. Lu, C. Wang, J. Qian, C. Ren, K. An, K. Wang, Target-driven switch-on fluorescence aptasensor for trace aflatoxin B1 determination based on highly fluorescent ternary CdZnTe quantum dots, Anal. Chim. Acta 1047 (2019) 163–171.
[23] X. Guo, F. Wen, N. Zheng, Q. Luo, H. Wang, H. Wang, S. Li, J. Wang, Development of an ultrasensitive aptasensor for the detection of aflatoxin B1, Biosens. Bioelectron. 56 (2014) 340–344.
[24] C. Wang, J. Qian, K. An, X. Lu, X. Huang, A semiconductor quantum dot-based ratiometric electrochemical aptasensor for the selective and reliable determination of aflatoxin B1, Analyst 144 (2019) 4772–4780.
[25] S.S. Wu, M. Wei, W. Wei, Y. Liu, S. Liu, Electrochemical aptasensor for aflatoxin B1 based on smart host-guest recognition of beta-cyclodextrin polymer, Biosens. Bioelectron. 129 (2019) 58–63.
[26] Y. Jia, G. Zhou, P. Liu, Z. Li, B. Yu, Recent development of aptamer sensors for the quantification of aflatoxin B1, Appl. Sci. 9 (2019) 2364.
[27] Y. Zhou, J. Zhi, The application of boron-doped diamond electrodes in amperometric biosensors, Talanta 79 (2009) 1189–1196.
[28] A. Kapałka, G. Fóti, C. Comninellis, The importance of electrode material in environmental electrochemistry: formation and reactivity of free hydroxyl radicals on boron-doped diamond electrodes, Electrochim. Acta 54 (2009) 2018–2023.
[29] S. Garcia-Segura, E.V. Dos Santos, C.A. Martinez-Huitle, Role of sp3/sp2 ratio on the electrocatalytic properties of boron-doped diamond electrodes: a mini review, Electrochem. Commun. 59 (2015) 52–55.
[30] Y.B. Ma, J.S. Liu, H.D. Li, Diamond-based electrochemical aptasensor realizing a femtomolar detection limit of bisphenol A, Biosens. Bioelectron. 92 (2017) 21–25.
[31] A. Chrouda, A. Sbartai, A. Baraket, L. Renaud, A. Maaref, N. Jaffrezic-Renault, An aptasensor for ochratoxin A based on grafting of polyethylene glycol on a boron-doped diamond microcell, Anal. Biochem. 488 (2015) 36–44.
[32] H. Ke, M. Liu, L. Zhuang, Z. Li, L. Fan, G. Zhao, A fetomolar level 17 beta-estradiol electrochemical aptasensor constructed on hierachical dendritic gold modified boron-doped diamond electrode, Electrochim. Acta 137 (2014) 146–153.
[33] G. Evtugyn, A. Porfireva, V. Stepanova, R. Sitdikov, I. Stoikov, D. Nikolelis, T. Hianik, Electrochemical aptasensor based on polycarboxylic macrocycle modified with neutral red for aflatoxin B1 detection, Electroanalysis 26 (2014) 2100–2109.
[34] H.D. Li, T. Zhang, L.A. Li, X. Lü, B. Li, Z.S. Jin, G.T. Zou, Investigation on crystalline structure, boron distribution, and residual stresses in freestanding boron-doped CVD diamond films, J. Cryst. Growth 312 (2010) 1986–1991.
[35] J.D. Qiu, R. Wang, R.P. Liang, X.H. Xia, Electrochemically deposited nanocomposite film of CS-Fc/Au NPs/GOx for glucose biosensor application, Biosens. Bioelectron. 24 (2009) 2920–2925.
[36] J. Shabani Shayeh, A. Ehsani, M.R. Ganjali, P. Norouzi, B. Jaleh, Conductive polymer/reduced graphene oxide/Au nano particles as efficient composite materials in electrochemical supercapacitors, Appl. Surf. Sci. 353 (2015) 594–599.
[37] G. Pelossof, R. Tel-Vered, S. Shimron, I. Willner, Controlling interfacial electron transfer and electrocatalysis by pH- or ion-switchable DNA monolayer-modified electrodes, Chem. Sci. 4 (2013) 1137.
[38] X. Yuan, N. Gao, X. Gao, D. Qiu, R. Xu, Z. Sun, Z. Jiang, J. Liu, H. Li, Nanopyramid boron-doped diamond electrode realizing nanomolar detection limit of 4-nonylphenol, Sensor. Actuator. B Chem. 281 (2019) 830–836.
[39] X. Chen, Y. Wang, J. Zhou, W. Yan, X. Li, J.-J. Zhu, Electrochemical impedance immunosensor based on three-dimensionally ordered macroporous gold film, Anal. Chem. 80 (2008) 2133–2140.
[40] X. Ma, W. Wang, X. Chen, Y. Xia, S. Wu, N. Duan, Z. Wang, Selection, identification, and application of Aflatoxin B1 aptamer, Eur. Food Res. Technol. 238 (2014) 919–925.
[41] L.G. Carrascosa, A.A.I. Sina, R. Palanisamy, B. Sepulveda, M.A. Otte, S. Rauf, M.J. Shiddiky, M. Trau, Molecular inversion probe-based SPR biosensing for specific, label-free and real-time detection of regional DNA methylation, Chem. Commun. 50 (2014) 3585–3588.